THE EUROPEAN
PHYSICAL JOURNAL C

χ_{c1} and χ_{c2} polarization as a probe of color octet channel

S. P. Baranov[1], **A. V. Lipatov**[2,3,a]

[1] P.N. Lebedev Institute of Physics, Moscow 119991, Russia
[2] Skobeltsyn Institute of Nuclear Physics, Lomonosov Moscow State University, Moscow 119991, Russia
[3] Joint Institute for Nuclear Research, 141980 Dubna, Moscow Region, Russia

Abstract We analyze joint LHC data on the production of χ_{c1} and χ_{c2} mesons together with the polarization data obtained very recently by the CMS Collaboration at $\sqrt{s} = 8$ TeV. Our consideration is based on the k_T-factorization approach and nonrelativistic QCD formalism for the formation of bound states. The observed polar anisotropy of χ_{c1} and χ_{c2} decays can be described as a combined effect of the color-singlet and color-octet contributions. We extract the corresponding long-distance matrix elements from the fits. Our fits point to unequal color singlet wave functions for χ_{c1} and χ_{c2} states.

Very recently, the CMS Collaboration reported on the first measurement [1] of the polarization of prompt χ_{c1} and χ_{c2} mesons produced in pp collisions at the energy $\sqrt{s} = 8$ TeV. The polarizations were measured in the decay chain $\chi_c \to J/\psi + \gamma$, $J/\psi \to \mu^+\mu^-$ in the J/ψ helicity frame through studying the ratio of the yields χ_{c2} to χ_{c1} as a function of the positive muon polar and azimuthal angles in three bins of J/ψ transverse momentum. No difference was seen between the χ_{c1} and χ_{c2} states in the azimuthal distributions, whereas they showed significantly different polar anisotropies. Thus, at least one of these mesons should have been strongly polarized along the helicity axis [1]. This result contrasts with the unpolarized scenario observed for direct S-wave charmonia (J/ψ, ψ') and bottomonia $\Upsilon(nS)$ at the LHC over a wide transverse momentum range (see, for example, [2,3] and references therein).

A commonly accepted framework for the description of heavy quarkonia production and decay is the non-relativistic Quantum Chromodynamic (NRQCD) [4–6]. The perturbatively calculated cross sections for the short distance production of a heavy quark pair $Q\bar{Q}$ in an intermediate state $^{2S+1}L_J^{(a)}$ with spin S, orbital angular momentum L, total angular momentum J, and color representation a are complemented with long distance matrix elements (LDMEs) which

describe non-perturbative transitions of the intermediate $Q\bar{Q}$ pairs into a physical meson via soft gluon radiation. The NRQCD calculations at next-to-leading order (NLO) successfully describe the charmonia J/ψ, ψ', χ_{cJ} [7–14] and bottomonia $\Upsilon(nS)$, $\chi_{bJ}(mP)$ [15–19] transverse momenta distributions and agree well with the first CMS data [1] on the χ_{cJ} polarization at the LHC.

However, NRQCD has a long-standing challenge in the S-wave charmonia polarization (see, for example, discussions [20–22] and references therein). The description of η_c production data [23] reported recently by the LHCb Collaboration also turned out to be rather puzzling [24,25]. NRQCD faces certain problems in describing $J/\psi + X_{\text{non}-c\bar{c}}$ production at B factories, J/ψ photoproduction at HERA, and the p_T integrated (or total) cross section including its energy dependence. The worst discrepancies show up in comparisons of the different classes of the data, e.g., hadroproduction versus photoproduction, polarization versus p_T distributions, total cross sections versus differential cross sections, etc. The reader can find more discussion in an extensive review [22]. So, at present, the overall situation is still far from through understanding, and further theoretical studies are still an urgent task.

Part of the problems were solved with the k_T-factorization approach. Thanks to the initial gluon transverse momentum k_T, the final state p_T spectrum becomes harder, and so, less color-octet contribution is needed to fit the data. This removes the old conflict between the photo- and hadroproduction fits. It is quite similar to what one has in the colliear factorization with initial state radiation shower (see [26]). The data coming from B factories are still an open question.

A possible solution to the J/ψ non polarization problem was proposed [27]. There, the classical multipole radiation theory is employed to describe nonperturbative transformations of the color octet (CO) quark pairs produced in hard subprocesses into observed final state quarkonia. The key assumption made [27] is that the intermediate color-octet

[a] e-mail: lipatov@theory.sinp.msu.ru (corresponding author)

states are enough long living to be considered as real physical states with definite total angular momentum J and its projection J_z, rather than fictituous states with definite L_z and S_z. This immediately induces nonconservation of L_z and S_z in the color-electric dipole transitions (and in all other transitions as well; L_z ans S_z melt together to form J and J_z and do no longer remember who was who). As a consequence, the strong transverse polarization of $^3S_1^{[8]}$ state produced in hard subprocess gets lost (to zero) after two E1 gluon emissions $^3S_1^{[8]} \to {}^3P_J^{[8]} \to J/\psi$. This scheme successfully describes the observed S-wave charmonia [28] and bottomonia [29,30] polarizations. As a byproduct it removes tension with the η_c production data [31]. The depolarization scenario [27] shows no need in the $^1S_0^{[8]}$ contribution in J/ψ production. That means, accordingly, no $^3S_1^{[8]}$ contribution in the η_c production, an HQSS counterpart of the former channel.

The main goal of our present note is to extend the approach [27] to the first and very new CMS data [1] on χ_{cJ} polarization. We propose a method to implement these data into the LDMEs fit procedure, thus refining the previously extracted LDMEs for χ_{cJ} mesons. Our study sheds light on the role of CO contributions which were thought unnecessary or even unwanted [13] for χ_{cJ} p_T spectra or their relative rates $\sigma(\chi_{c2})/\sigma(\chi_{c1})$, but which reveal now in the measured polar anisotropies. To preserve the consistency with our previous studies [28–31], we follow mostly the same steps and employ the k_T-factorization approach [32–35] to produce the $c\bar{c}$ pair in the hard parton scattering. The newly added calculations are only for the feeddown contributions from ψ' radiative decays.

For the reader's convenience, we briefly recall the calculation details. Our consideration is based on the off-shell gluon-gluon fusion subprocess that represents the true leading order (LO) in QCD:

$$g^*(k_1) + g^*(k_2) \to c\bar{c}\left[^3P_J^{[1]}, {}^3S_1^{[8]}\right](p) \tag{1}$$

for χ_{cJ} mesons with $J = 0, 1, 2$. The four-momenta of all particles are indicated in the parentheses and the possible intermediate states of the $c\bar{c}$ pair are listed in the brackets. The initial off-shell gluons have non-zero transverse momenta $k_{1T}^2 = -\mathbf{k}_{1T}^2 \neq 0$, $k_{2T}^2 = -\mathbf{k}_{2T}^2 \neq 0$ and, consequently, an admixture of longitudinal component in the polarization vectors. According to the k_T-factorization prescription [34, 35], the gluon spin density matrix is taken in the form

$$\sum \epsilon^\mu \epsilon^{*\nu} = \frac{\mathbf{k}_T^\mu \mathbf{k}_T^\nu}{\mathbf{k}_T^2}, \tag{2}$$

where $\mathbf{k}_T$ is the component of the gluon momentum perpendicular to the beam axis. In the collinear limit, where $\mathbf{k}_T^2 \to 0$, this expression converges to the ordinary $-g^{\mu\nu}$

after averaging over the gluon azimuthal angle. In all other respects, we follow the standard QCD Feynman rules. The hard production amplitudes contain spin and color projection operators [36–39] that guarantee the proper quantum numbers of the state under consideration. The respective cross section

$$\sigma(pp \to \chi_{cJ} + X)$$
$$= \int \frac{2\pi}{x_1 x_2 s F} f_g(x_1, \mathbf{k}_{1T}^2, \mu^2) f_g(x_2, \mathbf{k}_{2T}^2), \mu^2) \times$$
$$\times |\bar{\mathcal{A}}(g^* + g^* \to \chi_{cJ})|^2 d\mathbf{k}_{1T}^2 d\mathbf{k}_{2T}^2 dy \frac{d\phi_1}{2\pi} \frac{d\phi_2}{2\pi}, \tag{3}$$

where ϕ_1 and ϕ_2 are the azimuthal angles of incoming off-shell gluons carrying the longitudinal momentum fractions x_1 and x_2, y is the rapidity of produced χ_{cJ} mesons, F is the off-shell flux factor [40], and $f_g(x, \mathbf{k}_T^2, \mu^2)$ is the transverse momentum dependent (TMD, or unintegrated) gluon density function. More details can be found in our previous papers [28–31]. Presently, all of the above formalism is implemented into the newly developed Monte-Carlo event generator PEGASUS [41].

As usual, we have tried several sets of TMD gluon densities in a proton. Three of them, namely, A0 [42], JH'2013 set 1 and JH'2013 set 2 [43] have been obtained from Catani–Ciafaloni–Fiorani–Marchesini (CCFM) evolution equation [44–47], where the input parametrizations (used as boundary conditions) have been fitted to the proton structure function $F_2(x, Q^2)$. Besides that, we have tested a TMD gluon distribution obtained within the Kimber–Martin–Ryskin (KMR) prescription [48–50], which provides a method to construct the TMD parton densities from the conventional (collinear) ones [1]. Following [52], we set the meson masses to $m(\chi_{c1}) = 3.51$ GeV, $m(\chi_{c2}) = 3.56$ GeV, $m(J/\psi) = 3.096$ GeV and branching fractions $B(\chi_{c1} \to J/\psi\gamma) = 33.9\%$, $B(\chi_{c2} \to J/\psi\gamma) = 19.2\%$ and $B(J/\psi \to \mu^+\mu^-) = 5.961\%$ everywhere in the calculations below. When evaluating the feeddown contributions from ψ' radiative decays, $\psi' \to \chi_{cJ} + \gamma$, we set $m(\psi') = 3.69$ GeV, $B(\psi' \to \chi_{c1}\gamma) = 9.75\%$ and $B(\psi' \to \chi_{c2}\gamma) = 9.52\%$. The parton level calculations have been performed using the Monte-Carlo generator PEGASUS.

As it was mentioned above, to determine the LDMEs of χ_{cJ} mesons a global fit to the χ_{cJ} production data at the LHC was performed [28]. The data on the χ_{c1} and χ_{c2} transverse momentum distributions provided by ATLAS Collaboration [53] at $\sqrt{s} = 7$ TeV and the production rates $\sigma(\chi_{c2})/\sigma(\chi_{c1})$ reported by CMS [54], ATLAS [53] and LHCb [55,56] Collaborations were included in the fit. Here we extend our previous consideration and incorporate it with the first data [1] on the χ_{c1} and χ_{c2} polarization collected by CMS Collaboration at $\sqrt{s} = 8$ TeV. In the original CMS analysis, the χ_{cJ} polarization was extracted from the (di)muon angular distri-

---

[1] For the input, we have used LO MMHT'2014 set [51].

butions in the helicity frame of the daughter J/ψ meson. The latter is parametrized as

$$\frac{d\sigma}{d\cos\theta^* d\phi^*} \sim \frac{1}{3 + \lambda_\theta}$$
$$\left(1 + \lambda_\theta \cos^2\theta^* + \lambda_\phi \sin^2\theta^* \cos 2\phi^* \right.$$
$$\left. + \lambda_{\theta\phi} \sin 2\theta^* \cos\phi^* \right), \tag{4}$$

where θ^* and ϕ^* are the positive muon polar and azimuthal angles, so that the χ_{cJ} angular momentum is encoded in the polarization parameters λ_θ, λ_ϕ and $\lambda_{\theta\phi}$. The ratio of the yields $\sigma(\chi_{c2})/\sigma(\chi_{c1})$ has been measured as a function of $\cos\theta^*$ and ϕ^* in three different regions of J/ψ transverse momentum, $8 < p_T < 12$ GeV, $12 < p_T < 18$ GeV and $18 < p_T < 30$ GeV, thus leading to a simple correlation between the $\lambda_\theta^{\chi_{c1}}$ and $\lambda_\theta^{\chi_{c2}}$ parameters:

$$\lambda_\theta^{\chi_{c2}} = \left(-0.94 + 0.90\lambda_\theta^{\chi_{c1}}\right) \pm \left(0.51 + 0.05\lambda_\theta^{\chi_{c1}}\right),$$
$$8 < p_T < 12 \text{ GeV}, \tag{5}$$
$$\lambda_\theta^{\chi_{c2}} = \left(-0.76 + 0.80\lambda_\theta^{\chi_{c1}}\right) \pm \left(0.26 + 0.05\lambda_\theta^{\chi_{c1}}\right),$$
$$12 < p_T < 18 \text{ GeV}, \tag{6}$$
$$\lambda_\theta^{\chi_{c2}} = \left(-0.78 + 0.77\lambda_\theta^{\chi_{c1}}\right) \pm \left(0.26 + 0.06\lambda_\theta^{\chi_{c1}}\right),$$
$$18 < p_T < 30 \text{ GeV}. \tag{7}$$

Our main idea is to extract the LDME for $^3S_1^{[8]}$ contributions, $\mathcal{O}^{\chi_{c0}}\left[^3S_1^{[8]}\right]$, from the polarization data, since it can only be poorly determined from the measured χ_{cJ} transverse momentum distributions. To be precise, a good description of the latter can be achieved for a widely ranging $\mathcal{O}^{\chi_{c0}}\left[^3S_1^{[8]}\right]$, always with reasonably good $\chi^2/d.o.f.$ (see, for example, [12–14]). Moreover, its zero value is even preferable for the production rate ratio $\sigma(\chi_{c2})/\sigma(\chi_{c1})$ [13]. However, the reported production rates plotted as functions of $\cos\theta^*$ and ϕ^* have free (indefinite) normalization [57] and thus it is difficult to immediately implement them into the LDMEs fitting procedure. Therefore, we had to use the parametrizations (5)–(7) for our purposes.

Our fitting procedure is the following. First, we performed a fit of the χ_{c1} and χ_{c2} transverse momentum distributions and their relative production rates $\sigma(\chi_{c2})/\sigma(\chi_{c1})$ and determined the values of CS wave functions of χ_{cJ} mesons at the origin, $|\mathcal{R}'^{\chi_{c1}}(0)|^2$ and $|\mathcal{R}'^{\chi_{c2}}(0)|^2$, for a (large) number of fixed guessed $\mathcal{O}^{\chi_{c0}}\left[^3S_1^{[8]}\right]$ values in the range $10^{-4} < \mathcal{O}^{\chi_{c0}}\left[^3S_1^{[8]}\right] < 10^{-3}$ GeV^3. At this step we employ the fitting algorithm implemented in the GNUPLOT package [58]. Following [59], we considered the CS wave functions as independent (not necessarily identical) free parameters. We understand that doing so is at odds with the Heavy Quark Effective Theory (HQET) and Heavy Quark Spin Symmetry (HQSS). We think however that HQSS predictions must not be taken for granted. In particular, HQSS tells that the masses of χ_{cJ} states must be equal for all J. In reality, they are differ-

ent. The reason may be seen in the spin–orbital interactions or in radiative corrections which can be large. But the goal of the present paper is not in giving an explanation for the origin of HQSS violations. Our earlier attempt [59] to preserve HQSS shows that it can hardly be possible. Here we try two alternative scenarios. We admit HQSS violation either solely for the color singlet states ("fit I"), or for both color singlet and color octet states ("fit II"). In the latter case, the color octet NMEs are also treated as independent parameters not related to each other through the $(2J+1)$ factor.

The published data on the ratio of the cross sections $\sigma(\chi_{c2})/\sigma(\chi_{c1})$ rely on the hypothesis of unpolarised mesons (with uniform angular distributions of their decay products). Now we know, *a posteriori*, that the mesons are polarised. Among the options for which the experimental collaborations have estimated the correction factors, our χ_{c1} and χ_{c2} helicities lie somewhere in between the "(0, 0)" and "(unpolarized, unpolarised)" cases. In the utmost "(0, 0)" case, the $\sigma(\chi_{c2})/\sigma(\chi_{c1})$ ratio has to be corrected by a factor of about 0.75 (see Table 4 in [54], Table 2 in [55], Table 2 in [56]). The real polarization is large, but not fully "(0, 0)" and gradually decreases at high p_T (due to increasing color-octet contributions); the correction factor should then go closer to 1. The dependence of the correction factor on the polarization strength is nonlinear and does not allow simple interpolation. In such a situation, we cannot calculate the proper correction for the $\sigma(\chi_{c2})/\sigma(\chi_{c1})$ ratio to perform a rigorous fit. So, we still use the "(unpolarized, unpolarised)" hypothesis, though understand that it is rather approximate, and take this uncertainty as part of the ultimate uncertainty band.

Having the first step of the fitting procedure finished, we collect the events simulated in the kinematical region defined by the CMS measurement [1] and generate the decay muon angular distributions according to the production and decay matrix elements. By applying a three-parametric fit based on (4), we determine the polarization parameters $\lambda_\theta^{\chi_{c1}}$ and $\lambda_\theta^{\chi_{c2}}$ as functions of $\mathcal{O}^{\chi_{c0}}\left[^3S_1^{[8]}\right]$ (see Fig. 1, where our results for "fit I" scenario are shown). We find that the dependence of these parameters on $\mathcal{O}^{\chi_{c0}}\left[^3S_1^{[8]}\right]$ is essential and therefore can be used to extract the latter from the data. One can see that χ_{c1} and χ_{c2} mesons show significantly different (large and opposite) polar anisotropies, $\lambda_\theta^{\chi_{c1}} > 0$ and $\lambda_\theta^{\chi_{c2}} < 0$, which smoothly decrease when $\mathcal{O}^{\chi_{c0}}\left[^3S_1^{[8]}\right]$ grows[2]. It is important to remind that each of the considered $\mathcal{O}^{\chi_{c0}}\left[^3S_1^{[8]}\right]$ values provides already a good fit to the p_T spectra: each value of $\mathcal{O}^{\chi_{c0}}\left[^3S_1^{[8]}\right]$ is associated with a respective set of commonly fitted color-singlet LDMEs. Now, using the relations (5)–(7) between $\lambda_\theta^{\chi_{c1}}$ and $\lambda_\theta^{\chi_{c2}}$ (shown by dashed curves in Fig. 1) one can easily extract $\mathcal{O}^{\chi_{c0}}\left[^3S_1^{[8]}\right]$ for each of the three p_T

---

[2] The polarization of χ_{cJ} mesons in the collinear scheme has been investigated in [60,61].

Fig. 1 Polarization parameters $\lambda_\theta^{\chi_{c1}}$ and $\lambda_\theta^{\chi_{c2}}$ calculated as a functions of $\mathcal{O}^{\chi_{c0}}\left[^3S_1^{[8]}\right]$ in the helicity frame at $|y(J/\psi)| < 1.2$ and $\sqrt{s} = 8$ TeV in three different p_T regions. Solid green and yellow curves represent the results of exact and approximated (when the intermediate $^3S_1^{[8]}$ state is taken unpolarized) calculations. Dashed curves correspond to the correlations (5)–(7) reported by the CMS Collaboration [1]. Everywhere, the JH'2013 set 2 gluon density is used. The color-octet LDMEs are assumed to obey HQSS ("fit I" scenario)
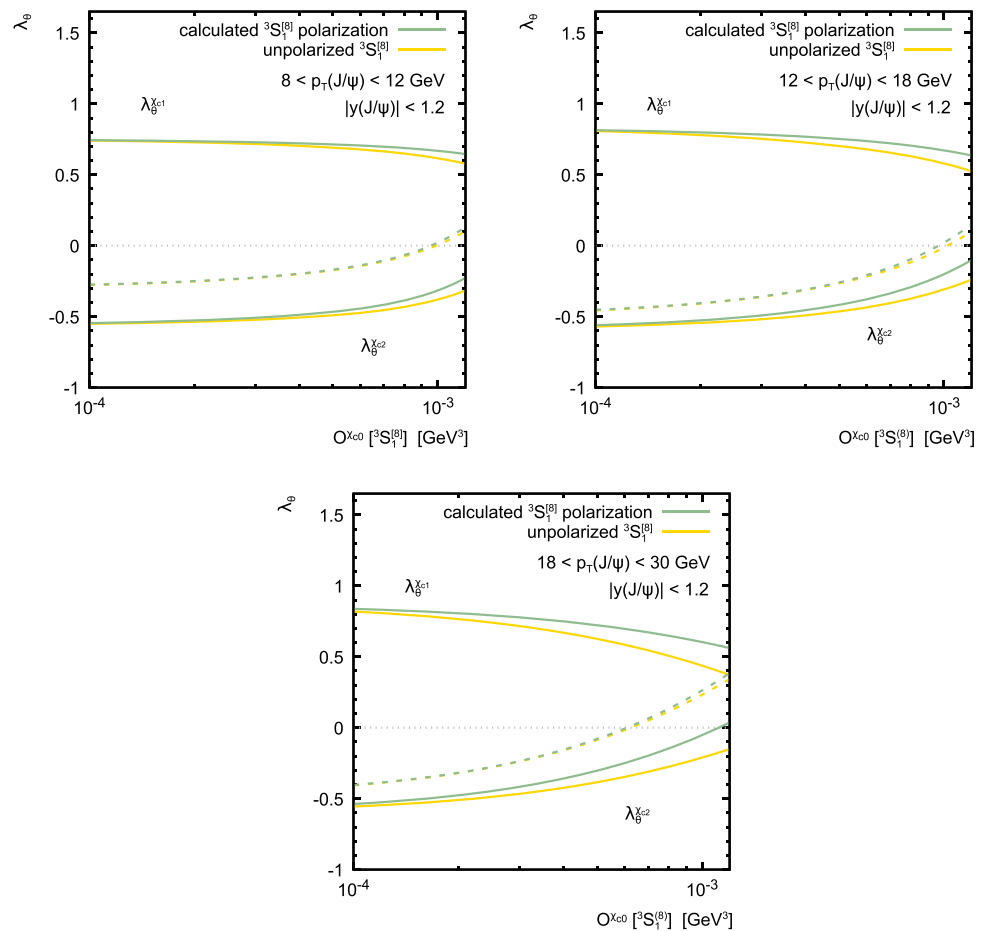
regions. The same method is used in both scenarios ("fit I" and "fit II"). Finally, the mean-square average is taken as the fitted values. Thus, this provides us with a complementary way to determine the LDMEs for χ_{cJ} mesons from the polarization data.

It is interesting to note that the determined values of $\mathcal{O}^{\chi_{c0}}\left[^3S_1^{[8]}\right]$ almost do not depend on the exact polarization of $^3S_1^{[8]}$ contributions in the CO channel. This can be easily understood because χ_{c1} and χ_{c2} mesons from the $^3S_1^{[8]}$ intermediate state produce very close J/ψ polarization, while the measured polar asymmetry is driven by the difference $\lambda_\theta^{\chi_{c1}} - \lambda_\theta^{\chi_{c2}}$. To illustrate it, we have repeated the calculations treating the $^3S_1^{[8]}$ contributions as unpolarized (yellow curves in Fig. 1). As one can see, the correlations (5)–(7) obtained in this toy approximation practically coincide with exact calculations.

The mean-square average of the extracted $\mathcal{O}^{\chi_{c0}}\left[^3S_1^{[8]}\right]$ values and the corresponding CS wave functions at the origin $|\mathcal{R}'^{\chi_{c1}}(0)|^2$ and $|\mathcal{R}'^{\chi_{c2}}(0)|^2$ are shown in Tables 1 ("fit I") and 2 ("fit II") for all tested TMD gluon densities. The relevant uncertainties are estimated in the conventional way using Student's t-distribution at the confidence level $P = 95\%$. For comparison, we also present the LDMEs obtained in the NLO NRQCD by other authors [13,14]. Both our fit scenar-

ios show unequal values for the χ_{c1} and χ_{c2} wave functions with the ratio $|\mathcal{R}'^{\chi_{c1}}(0)|^2/|\mathcal{R}'^{\chi_{c2}}(0)|^2 \sim 3 - 4$ ("fit I") or $1.3 - 2.5$ ("fit II") for all considered TMD gluon densities in a proton. "Fit II" moderates the difference between the color singlet wave functions as larger part of the χ_{c1} yield is now contained in the color octet channel. Thus, we interpret the available LHC data as supporting their unequal values, that qualitatively agrees with the previous results [28,59]. This leads to a different role of CO contributions to the χ_{c1} and χ_{c2} production cross sections. So, the χ_{c1} production is dominated by the CS contributions, whereas CO terms are more important for χ_{c2} mesons (see Fig. 2).

Of course, we have to keep in mind that the distinction between the color-singlet and color-octet contributions is conditional and is only valid within our LO scheme. In general, this distinction is related to the cancellation procedure between the virtual (loop) and real (tree) infrared divergences and is controlled by the arbitrary NRQCD scale μ_Λ.

All the LHC data involved in the fits are compared with our predictions in Figs. 2, 3 and 4. The green shaded bands represent the theoretical uncertainties of our calculations (responding to JH'2013 set 2 gluon density), which include both the scale uncertainties and the ones coming from the LDMEs fitting procedure. To estimate the scale uncertain-

Fig. 2 The prompt χ_{c1} and χ_{c2} production cross sections in pp collisions at $\sqrt{s} = 7$ TeV as a function of their transverse momenta. On left panels, the predictions obtained with different TMD gluon densities in a proton are presented. On right panels, the contributions from direct $^3P_J^{[1]}$, $^3S_1^{[8]}$ and feeddown production mechanisms are shown separately (the JH'2013 set 2 gluon distribution and "fit I" scenario were used for illustration). The experimental data are from ATLAS [53]
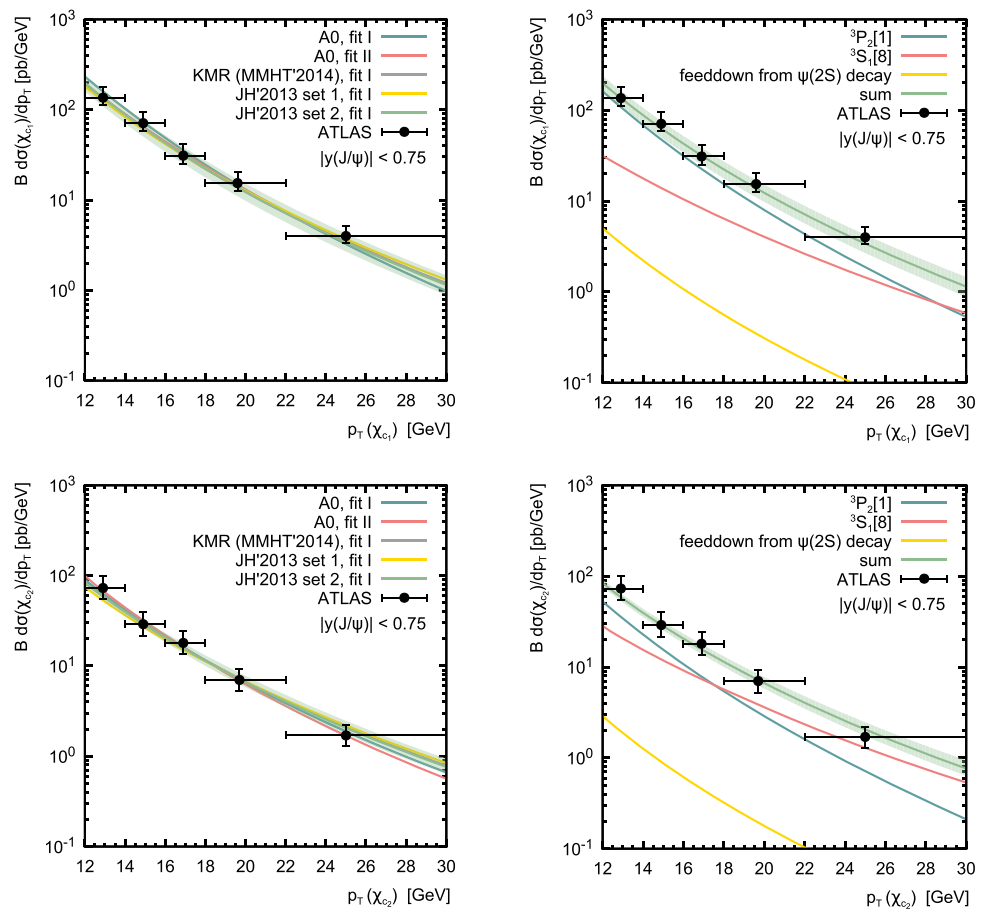
Fig. 3 The prompt χ_{c1} and χ_{c2} production cross sections in pp collisions at $\sqrt{s} = 7$ TeV as a function of decay J/ψ transverse momenta. Notation of all curves is the same as in Fig. 2. The experimental data are from ATLAS [53]
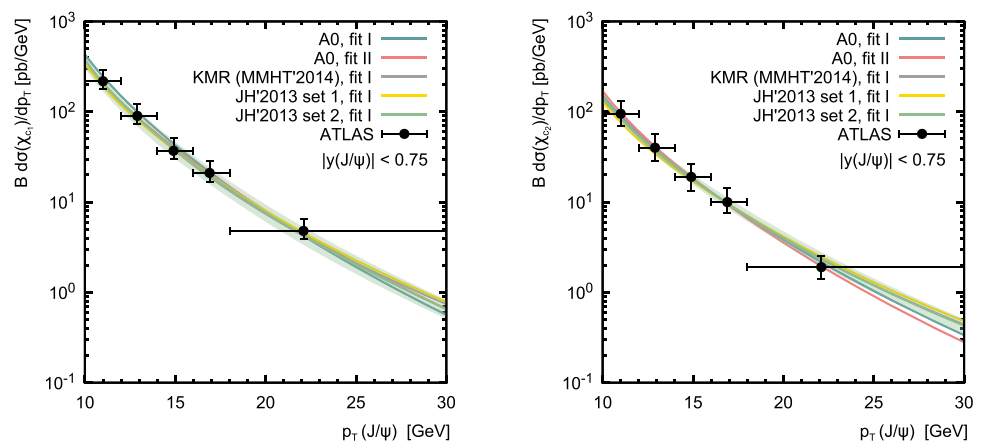
ties, the standard variations in the scale (by a factor of 2) were applied through replacing the JH'2013 set 2 gluon density with JH'2013 set 2+, or with JH'2013 set 2−, respectively. This was done to preserve the intrinsic correspondence between the TMD set and scale used in the evolution equation (see [43] for more information). We have achieved quite a nice agreement between our calculations and available LHC data. In particular, we obtained a simultaneous description of the transverse momentum distributions and the relative production rates $\sigma(\chi_{c2})/\sigma(\chi_{c1})$. There are some deviations

from the data at low p_T region, where, however, an accurate treatment of large logarithms $\ln m(\chi_{cJ})/p_T$ and other nonperturbative effects is needed.

The $\lambda_\theta^{\chi_{c2}}$ values extracted according to (5)–(7) when $\lambda_\theta^{\chi_{c1}}$ is fixed to our predictions are shown in Fig. 5. As one can see, our fit well agrees with the experimentally determined correlations between $\lambda_\theta^{\chi_{c1}}$ and $\lambda_\theta^{\chi_{c2}}$. The predicted $\lambda_\theta^{\chi_{cJ}}$ values are practically independent on the TMD gluon density and are close to the reported NLO NRQCD results [1].

Fig. 4 The relative production rate $\sigma(\chi_{c2})/\sigma(\chi_{c1})$ calculated as a function of decay J/ψ transverse momentum at $\sqrt{s} = 7$ TeV. Notation of all curves is the same as in Fig. 2. The experimental data are from ATLAS [53], CMS [54] and LHCb [55,56]
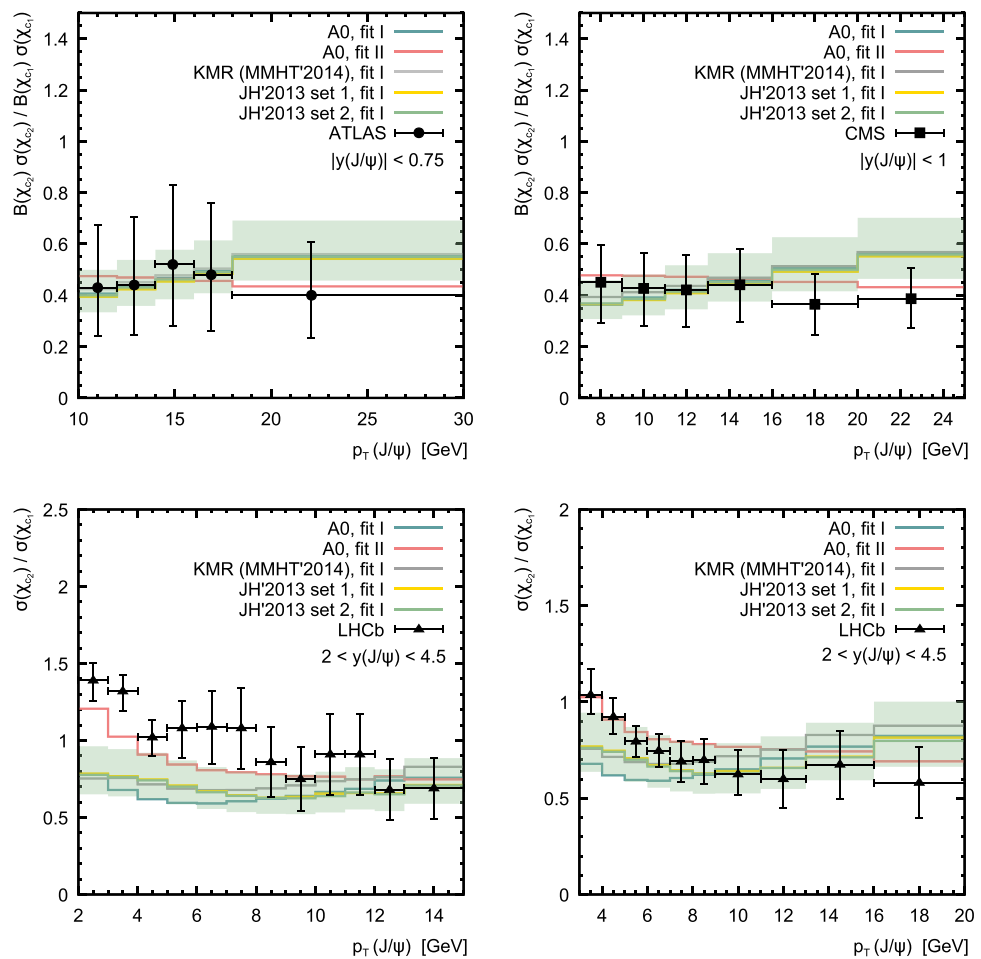
Fig. 5 The $\lambda_\theta^{\chi c2}$ values determined according to correlations (5)–(7) when the $\lambda_\theta^{\chi c1}$ is fixed to our predictions (left panel) or NRQCD ones (right panel). The NRQCD predictions are taken from CMS paper [1]
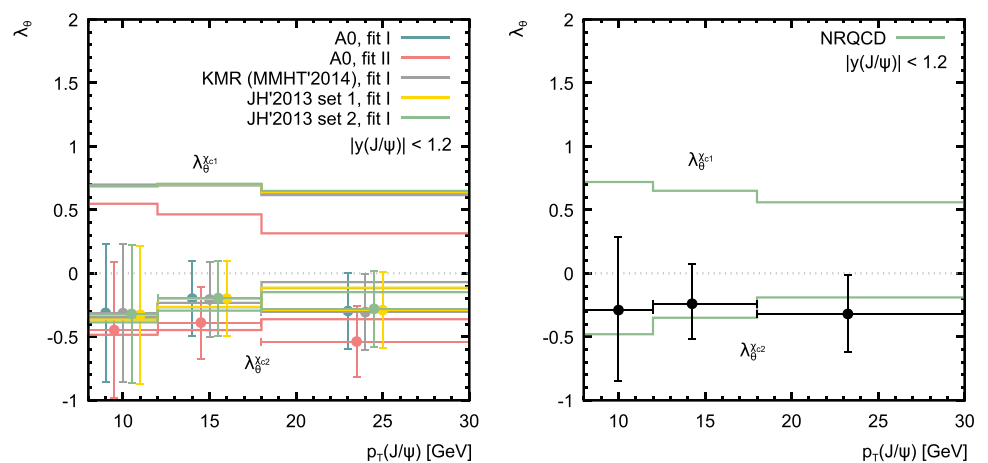
Having considered jointly the LHC data on the production and the polarization of χ_{c1} and χ_{c2} mesons we come to the following conclusions. Our first conclusion is that the presence of color octet contributions is indispensable. Taken solely, color octet contributions would produce too strong polar anisotropy. This remains valid irrespective of

the assumptions on the HQSS rules[3]. The second conclusion is that our fits point to unequal χ_{c1} and χ_{c2} color singlet wave functions. If we admit HQSS violation in the color octet sector as well, the fitted values of CO LDMEs also differ and

_____

[3] Once again, we have to remind that the interpretation of the different contributions as color singlets or color octets is only related to our particular computational framework and is of no meaning beyond this frame.

Table 1 The fitted values of LDMEs and CS wave functions at the origin (divided by the $2J + 1$ factor) for χ_{cJ} mesons. The color-octet LDMEs are assumed to obey HQSS ("fit I" scenario). The results obtained in the NLO NRQCD fits [13,14] are shown for comparison

Source	$\lvert\mathcal{R}'^{\chi_{c1}}(0)\rvert^2$/GeV^5	$\lvert\mathcal{R}'^{\chi_{c2}}(0)\rvert^2$/GeV^5	$\mathcal{O}^{\chi_{c0}}\left[{}^3S_1^{[8]}\right]$/GeV^3
A0	0.14 ± 0.03	0.0346 ± 0.0010	$(7.0 \pm 2.0) \times 10^{-4}$
JH'2013 set 1	0.17 ± 0.03	0.043 ± 0.004	$(7.0 \pm 2.0) \times 10^{-4}$
JH'2013 set 2	0.20 ± 0.04	0.0500 ± 0.0007	$(8.0 \pm 2.0) \times 10^{-4}$
KMR (MMHT'2014)	0.08 ± 0.02	0.026 ± 0.002	$(4.0 \pm 1.0) \times 10^{-4}$
NLO NRQCD fit [13]	0.35	0.35	4.4×10^{-4}
NLO NRQCD fit [14]	0.075	0.075	2.01×10^{-3}

Table 2 The fitted values of LDMEs and CS wave functions at the origin for χ_{cJ} mesons (divided by the $2J + 1$ factor). All LDMEs are considered independent ("fit II" scenario). The results obtained in the NLO NRQCD fits [13,14] are shown for comparison

Source	$\lvert\mathcal{R}'^{\chi_{c1}}(0)\rvert^2$/GeV^5	$\lvert\mathcal{R}'^{\chi_{c2}}(0)\rvert^2$/GeV^5	$\mathcal{O}^{\chi_{c1}}\left[{}^3S_1^{[8]}\right]$/GeV^3	$\mathcal{O}^{\chi_{c2}}\left[{}^3S_1^{[8]}\right]$/GeV^3
A0	0.11 ± 0.01	0.046 ± 0.004	$(1.2 \pm 0.8) \times 10^{-3}$	$(4.4 \pm 0.1) \times 10^{-4}$
JH'2013 set 1	0.10 ± 0.02	0.08 ± 0.01	$(1.7 \pm 0.5) \times 10^{-3}$	$(4.0 \pm 2.0) \times 10^{-5}$
JH'2013 set 2	0.148 ± 0.04	0.08 ± 0.01	$(1.7 \pm 0.9) \times 10^{-3}$	$(3.3 \pm 0.6) \times 10^{-4}$
KMR (MMHT'2014)	0.066 ± 0.001	0.042 ± 0.004	$(7.0 \pm 4.0) \times 10^{-4}$	$(1.8 \pm 0.9) \times 10^{-4}$
NLO NRQCD fit [13]	0.35	0.35	4.4×10^{-4}	4.4×10^{-4}
NLO NRQCD fit [14]	0.075	0.075	2.01×10^{-3}	2.01×10^{-3}

show the same trend giving emphasis to the χ_{c1} channel. Our third conclusion is that the data can be reasonably described with any of the examined TMD sets. The agreement is always good and does not give preference to any of them.

References

1. C.M.S. Collaboration, Phys. Rev. Lett. **124**, 162002 (2020)
2. C.M.S. Collaboration, Phys. Lett. B **727**, 381 (2013)
3. C.M.S. Collaboration, Phys. Rev. Lett. **110**, 081802 (2013)
4. G. Bodwin, E. Braaten, G. Lepage, Phys. Rev. D **51**, 1125 (1995)
5. P. Cho, A.K. Leibovich, Phys. Rev. D **53**, 150 (1996)
6. P. Cho, A.K. Leibovich, Phys. Rev. D **53**, 6203 (1996)
7. B. Gong, X.Q. Li, J.-X. Wang, Phys. Lett. B **673**, 197 (2009)
8. Y.-Q. Ma, K. Wang, K.-T. Chao, Phys. Rev. Lett. **106**, 042002 (2011)
9. M. Butenschön, B.A. Kniehl, Phys. Rev. Lett. **108**, 172002 (2012)
10. K.-T. Chao, Y.-Q. Ma, H.-S. Shao, K. Wang, Y.-J. Zhang, Phys. Rev. Lett. **108**, 242004 (2012)
11. B. Gong, L.-P. Wan, J.-X. Wang, H.-F. Zhang, Phys. Rev. Lett. **110**, 042002 (2013)
12. Y.-Q. Ma, K. Wang, K.-T. Chao, H.-F. Zhang, Phys. Rev. D **83**, 111503 (2011)
13. A.K. Likhoded, A.V. Luchinsky, S.V. Poslavsky, Phys. Rev. D **90**, 074021 (2014)
14. H.-F. Zhang, L. Yu, S.-X. Zhang, L. Jia, Phys. Rev. D **93**, 054033 (2016)
15. B. Gong, J.-X. Wang, H.-F. Zhang, Phys. Rev. D **83**, 114021 (2011)
16. K. Wang, Y.-Q. Ma, K.-T. Chao, Phys. Rev. D **85**, 114003 (2012)
17. B. Gong, L.-P. Wan, J.-X. Wang, H.-F. Zhang, Phys. Rev. Lett. **112**, 032001 (2014)
18. Y. Feng, B. Gong, L.-P. Wan, J.-X. Wang, H.-F. Zhang, Chin. Phys. C **39**, 123102 (2015)
19. H. Han, Y.-Q. Ma, C. Meng, H.-S. Shao, Y.-J. Zhang, K.-T. Chao, Phys. Rev. D **94**, 014028 (2016)
20. J.-P. Lansberg, H.-S. Shao, H.-F. Zhang, Phys. Lett. B **786**, 342 (2018)
21. Y. Feng, J. He, J.-P. Lansberg, H.-S. Shao, A. Usachov, H.-F. Zhang, Nucl. Phys. B **945**, 114662 (2019)
22. J.-P. Lansberg,. arXiv:1903.09185 [hep-ph]
23. LHCb Collaboration, Eur. Phys. J. C **75**, 311 (2015)
24. H.-F. Zhang, Z. Sun, W.-L. Sang, R. Li, Phys. Rev. Lett. **114**, 092006 (2015)
25. M. Butenschön, Z.G. He, B.A. Kniehl, Phys. Rev. Lett. **114**, 092004 (2015)

26. B.A. Kniehl, G. Kramer, Eur. Phys. J. C **6**, 493 (1999)
27. S.P. Baranov, Phys. Rev. D **93**, 054037 (2016)
28. S.P. Baranov, A.V. Lipatov, Phys. Rev. D **100**, 114021 (2019)
29. N.A. Abdulov, A.V. Lipatov, Eur. Phys. J. C **79**, 830 (2019)
30. N.A. Abdulov, A.V. Lipatov, Eur. Phys. J. C **80**, 486 (2020)
31. S.P. Baranov, A.V. Lipatov, Eur. Phys. J. C **79**, 621 (2019)
32. S. Catani, M. Ciafaloni, F. Hautmann, Nucl. Phys. B **366**, 135 (1991)
33. J.C. Collins, R.K. Ellis, Nucl. Phys. B **360**, 3 (1991)
34. L.V. Gribov, E.M. Levin, M.G. Ryskin, Phys. Rep. **100**, 1 (1983)
35. E.M. Levin, M.G. Ryskin, YuM Shabelsky, A.G. Shuvaev, Sov. J. Nucl. Phys. **53**, 657 (1991)
36. C.-H. Chang, Nucl. Phys. B **172**, 425 (1980)
37. E.L. Berger, D.L. Jones, Phys. Rev. D **23**, 1521 (1981)
38. R. Baier, R. Rückl, Phys. Lett. B **102**, 364 (1981)
39. S.S. Gershtein, A.K. Likhoded, S.R. Slabospitsky, Sov. J. Nucl. Phys. **34**, 128 (1981)
40. E. Bycling, K. Kajantie, *Particle Kinematics* (John Wiley and Sons, New York, 1973)
41. A.V. Lipatov, S.P. Baranov, M.A. Malyshev, Eur. Phys. J. C **80**, 330 (2020). https://theory.sinp.msu.ru/doku.php/pegasus/news
42. H. Jung, arXiv:hep-ph/0411287
43. F. Hautmann, H. Jung, Nucl. Phys. B **883**, 1 (2014)
44. M. Ciafaloni, Nucl. Phys. B **296**, 49 (1988)
45. S. Catani, F. Fiorani, G. Marchesini, Phys. Lett. B **234**, 339 (1990)
46. S. Catani, F. Fiorani, G. Marchesini, Nucl. Phys. B **336**, 18 (1990)
47. G. Marchesini, Nucl. Phys. B **445**, 49 (1995)
48. M.A. Kimber, A.D. Martin, M.G. Ryskin, Phys. Rev. D **63**, 114027 (2001)
49. A.D. Martin, M.G. Ryskin, G. Watt, Eur. Phys. J. C **31**, 73 (2003)
50. A.D. Martin, M.G. Ryskin, G. Watt, Eur. Phys. J. C **66**, 163 (2010)
51. L.A. Harland-Lang, A.D. Martin, P. Motylinski, R.S. Thorne, Eur. Phys. J. C **75**, 204 (2015)
52. P.D.G. Collaboration, Phys. Rev. D **98**, 030001 (2018)
53. ATLAS Collaboration, JHEP **07**, 154 (2014)
54. C.M.S. Collaboration, Eur. Phys. J. C **72**, 2251 (2012)
55. LHCb Collaboration, Phys. Lett. B **714**, 215 (2012)
56. LHCb Collaboration, JHEP **10**, 115 (2013)
57. C. Lourenco, P. Faccioli, Private communications
58. www.gnuplot.info
59. S.P. Baranov, Phys. Rev. D **83**, 034035 (2011)
60. B.A. Kniehl, G. Kramer, C.P. Palisoc, Phys. Rev. D **68**, 114002 (2003)
61. H.-S. Shao, Y.-Q. Ma, K. Wang, K.-T. Chao, Phys. Rev. Lett. **112**, 182003 (2014)